Lithium HalfSalen Complexes: Synthesis, Structural Characterization and Studies as Catalysts for racLactide Ring Opening Polymerization

EurJOC
European Journal of Organic Chemistry

Full Papers
doi.org/10.1002/ejoc.202100981

Chemistry Europe
European Chemical Societies Publishing

Special Collection

Lithium Half-Salen Complexes: Synthesis, Structural Characterization and Studies as Catalysts for *rac*-Lactide Ring-Opening Polymerization

Yali Zhou,[a] Gary S. Nichol,[a] and Jennifer A. Garden*[a]

Seven lithium complexes supported by sterically and electronically diverse phenoxyimine ligands were synthesized and characterized by X-ray diffraction, NMR spectroscopy and elemental microanalysis. These complexes show high activity ($k_{obs} \leq 7.43 \times 10^{-2}$ s^{-1}) for *rac*-lactide ring-opening polymerization (ROP) in the presence of co-initiator benzyl alcohol (BnOH), with the exception of **Li4** which features an unusual polymeric ladder structure. Overall, the catalyst activity correlates to the aggregation state; the catalysts with low aggregation states display increased propagation rates attributed to improved metal accessibility and kinetic mobility. The nature of the ligand substituents and solvent influence the catalyst aggregation in both the solid- and solution-state. While the lithium complexes can initiate *rac*-lactide ROP without BnOH, the addition of this co-initiator significantly increases the polymerization rate by switching the mechanism from a coordination-insertion to an activated monomer pathway, changing the resultant poly(lactic acid) architecture from cyclic to linear.

Introduction

The synthesis of biodegradable polymers derived from renewable sources is an attractive strategy to reduce societal reliance on petrochemical feedstocks and transition towards a circular economy.[1–3] Poly(lactic acid) (PLA) has gained particular interest, as it is readily sourced from sugar- or starch-rich biomass and has proven useful in packaging and medical applications.[4,5] Typically synthesized through ring-opening polymerization (ROP) of lactide (LA),[4] efficient PLA production requires the use of an appropriate catalyst. Different classes of catalysts have shown success, yet the industrial use of organocatalysts is currently limited by potential toxicity and economic concerns,[6,7] while enzymatic catalysts often give low yields and require long polymerization times with high catalyst loadings.[8,9] Organometallic catalysts are the most widely used, and efficient systems have been developed including those based on Al,[10–13] Zn,[14–16] or lanthanides.[17–19]

Most organometallic catalysts are proposed to operate through a coordination-insertion mechanism (Scheme 1, left), where LA coordination to a Lewis acidic metal center activates the monomer towards nucleophilic attack from a metal-alkoxide group (sometimes formed through *in situ* alcoholysis of a metal-alkyl precursor), resulting in LA ring-opening and enchainment.[20] Alternatively, an activated monomer mechanism can operate. While this pathway is generally observed with organocatalysts,[21] some organometallic catalysts have been reported to follow this route, which also features monomer activation by the metal center but with nucleophilic

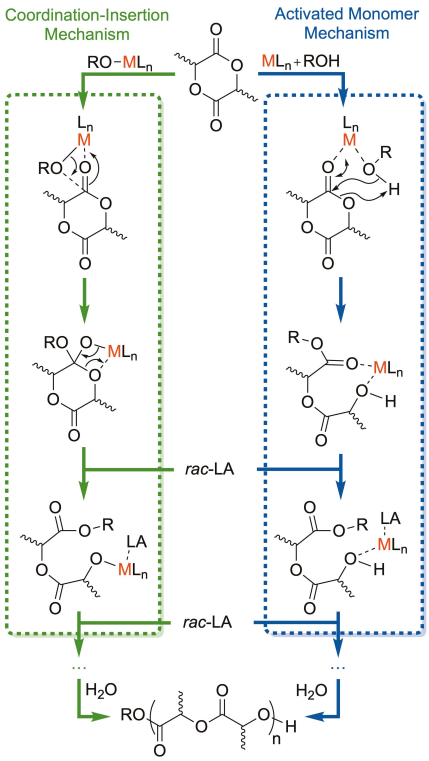

Scheme 1. Typical mechanisms for organometallic catalyzed LA ROP: Left, coordination-insertion; Right, activated monomer. L refers to ligand, M refers to metal and RO refers either to the initiator or the growing polymer chain.

[a] *Y. Zhou, Dr. G. S. Nichol, Dr. J. A. Garden*
EaStCHEM School of Chemistry
University of Edinburgh
Edinburgh, EH9 3FJ, UK
E-mail: j.garden@ed.ac.uk
http://www.chem.ed.ac.uk/staff/academic-staff/dr-jennifer-garden

Supporting information for this article is available on the WWW under https://doi.org/10.1002/ejoc.202100981

Part of the "EaSTCHEM" Virtual Institute Feature.

attack instead occurring from an exogeneous alcohol (Scheme 1, right).[22] With some catalyst systems, there is an ongoing debate as to whether the mechanism follows a coordination-insertion and/or an activated monomer pathway.[23] The metal is important for both routes, as strong Lewis acids can enhance LA coordination and thus improve propagation rates.[24] The nature of the catalyst metal-alkoxide bond is instructive; catalysts containing reactive metal-alkoxide units often follow a coordination-insertion pathway, while those with unreactive metal-alkoxide bonds generally observe an activated monomer mechanism.

Lithium complexes have shown great potential as LA ROP catalysts as lithium is highly Lewis acidic, inexpensive and non-toxic; the latter is an important benefit in preparing PLA for biomedical applications.[25–27] Simple lithium complexes such as butyllithium[28] and lithium tert-butoxide[28,29] are highly active for LA ROP but are generally accompanied by limited controllability and undesirable transesterification reactions. Tailored ligand design offers a route to improve the catalyst performance, and lithium complexes bearing bulky ligands such as aminephenolates[30] or azonaphtholates[26] have been reported as effective catalysts under mild conditions.

Phenoxyimine (half-salen) ligands are attractive precursors due to their straightforward preparation and tunable steric and electronic properties. These ligands display greater structural flexibility than the analogous salen ligands, complexes of which have shown high reactivity and selectivity in various polymerizations including LA,[31] ε-caprolactone,[6] and α-olefins.[32] Modification of the ligand substituents can lead to improved catalyst activities,[33] by enhancing the accessibility of the metal, as well as regulating the coordination number, geometry and the number of valence electrons, and some previous studies have shown that lithium phenoxyimine complexes give high activities in LA ROP.[31,34,35] This work reports the preparation of a series of half-salen lithium complexes bearing different substituents, and uncovers insights into the influence of electronics, sterics and aggregation state upon the performance in *rac*-LA ROP. Reactivity studies show how the presence of BnOH can modify the polymerization mechanism from coordination-insertion to activated-monomer, providing insight into the dynamic equilibria that occur in solution.

Results and Discussion

Synthesis and characterization

A series of lithium complexes were prepared in good yields through deprotonation of the relevant phenoxyimine ligands (**Li1**-**Li7**, Scheme 2). All seven complexes were characterized through multinuclear NMR spectroscopy and elemental microanalysis, and the solid-state structures of **Li1**-**Li5** and **Li7** were determined by single crystal X-ray diffraction studies. Single crystals of **Li1**, **Li3**-**Li5** and **Li7** were obtained from toluene solution, whilst **Li2** and **Li7** were crystallized from THF solution. **Li1** and **Li3** have previously been reported but were crystallized under different conditions.[34,36]

When crystallized from toluene solvent, complexes **Li1**, **Li5** and **Li7** were obtained as tetranuclear aggregates (Figures 1, S57 and S62). In contrast, **Li3** displays a dinuclear structure (Figure 2) whilst **Li4** has a polynuclear "ladder" structure (Figure 3).[37] Dinuclear **Li3**, bearing the most sterically bulky substituents [*ortho*-^{t}Bu-phenol and diisopropylphenyl (dipp)-N=C], has the lowest aggregation state. Featuring an almost planar Li_2O_2 core [dihedral angles $<11.1(1)°$], each Li coordinates to two phenolic oxygens, one imine nitrogen and the distorted tetrahedral geometry ($\tau_{4\text{-Li3}}=0.52$) is completed through an agostic interaction with the methyl-group of the ^{t}Bu substituent [Li1-H(C32) 2.066(2) Å; Li···H–C 127.0(2)°, Table S4]. The τ_4 factor is a geometric parameter that distinguishes a

Yali Zhou graduated with an MSc in Medicinal and Biological Chemistry from The University of Edinburgh (2018). In the same year she started her PhD studies under the supervision of Dr Jennifer Garden. Her research focuses on the design and synthesis of novel homo- and heterometallic catalysts for the ring-opening polymerization of cyclic esters.

A native of Sunderland, Gary Nichol obtained his PhD from Newcastle University followed by five years at The University of Arizona as the supervisor of the X-ray Diffraction Facility in the (then) Department of Chemistry. In 2011 he moved to Edinburgh University where he oversees a productive crystallography laboratory which includes regular, remote access to beam line I-19 at Diamond Light Source. He is a retired co-editor of Acta Crystallographica Section E.

Jennifer Garden received her MSc (1st Class Hons, 2010) and PhD (2014) from The University of Strathclyde, the latter under the direction of Prof. Robert Mulvey. This was followed by two years as a postdoctoral researcher in the group of Prof. Charlotte Williams at Imperial College London. In 2016, Jennifer moved to The University of Edinburgh as the first recipient of the Christina Miller Research Fellowship, which was followed by a Ramsay Memorial Trust Fellowship (2018–2020), L'Oréal-UNESCO for Women in Science UK & Ireland Fellowship (2019) and UKRI Future Leaders Fellowship (2020-present). Research in the Garden Group combines different fields of chemistry including catalyst development and sustainable polymer synthesis. Jennifer currently sits on the Editorial Advisory Board of ACS Macromolecules and her work has been recognized by awards including the Macro Group UK Young Researchers Medal and the RSC Dalton Division Sir Edward Frankland Fellowship.

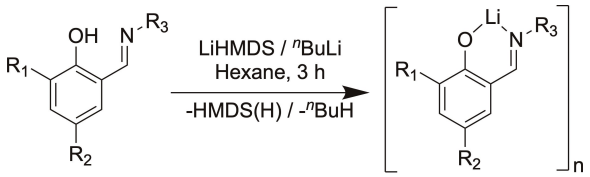

Li1: R_1=R_2=H; R_3=2,6-(^{i}Pr)$_2$C$_6$H$_3$, 85.0% yield
Li2: R_1=^{t}Bu; R_2=H; R_3=CH$_3$, 71.9% yield
Li3: R_1=^{t}Bu; R_2=H; R_3=2,6-(^{i}Pr)$_2$C$_6$H$_3$, 73.2% yield
Li4: R_1=Cl; R_2=H; R_3=CH$_3$, 87.6% yield
Li5: R_1=Cl; R_2=H; R_3=2,6-(^{i}Pr)$_2$C$_6$H$_3$, 53.5% yield
Li6: R_1=H; R_2=Cl; R_3=CH$_3$, 84.7% yield
Li7: R_1=H; R_2=Cl; R_3=2,6-(^{i}Pr)$_2$C$_6$H$_3$, 93.1% yield

Scheme 2. Synthesis of lithium half-salen complexes **Li1**-**Li7**.

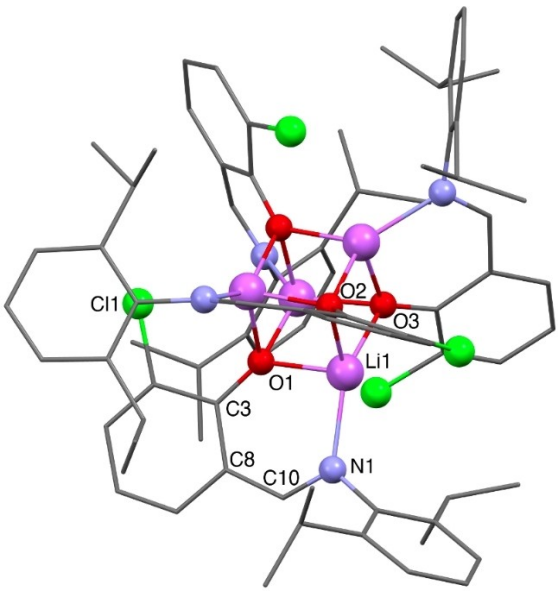

Figure 1. Typical molecular structure crystallized from toluene solvent (**Li5** shown as an example; refer to ESI for **Li1** and **Li7**). Hydrogen atoms have been omitted for clarity.

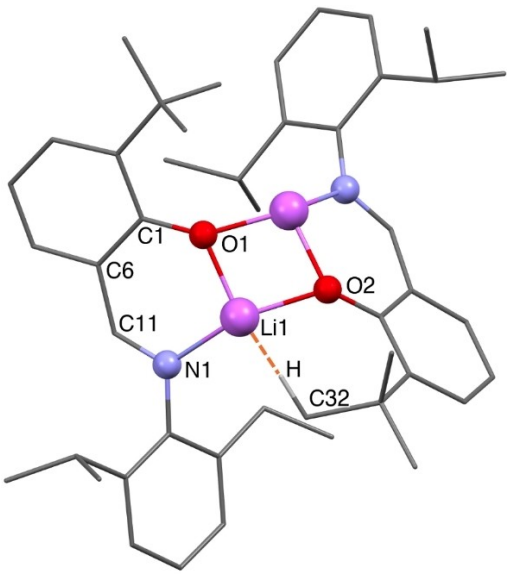

Figure 2. Molecular structure of **Li3** crystallized from toluene solvent. Hydrogen atoms have been omitted for clarity.

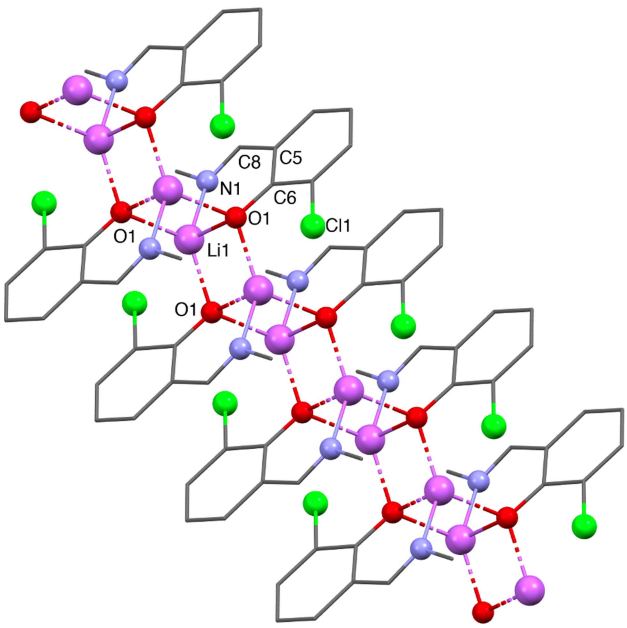

Figure 3. Polymeric chain structure of **Li4** crystallized from toluene solvent with the asymmetric unit and symmetry equivalent O1 labelled. Hydrogen atoms have been omitted for clarity.

perfect square planar geometry (τ_4 = 0) from a tetrahedral geometry (τ_4 = 1) for tetracoordinate metals.[38] To the best of our knowledge, the "ladder" structure of **Li4** is the first time this motif has been observed for a lithium-phenoxyimine complex. The ligand features sterically small substituents (*ortho*-Cl-phenol and Me-N=C), which facilitates π-π stacking between the aromatic phenol rings [distance = 3.613(5) Å], with the half-salen ligands arranged in parallel along the ladder rungs.[39] There is an electrostatic interaction between C–*Cl* and the nearest Li [Li–Cl 2.932(4) Å; shorter than the sum of radius of Li (1.82 Å) and Cl (1.75 Å)], which may help to stabilize the ladder structure. The distance between C–*Cl* and the nearest alkyl –*H* of the adjacent ring ranges from 2.383(3) to 4.545(3) Å; while weak, these H bonding/electrostatic interactions could possibly also contribute to stabilization of the ladder structure.[40] Consecutive four-membered Li_2O_2 rings are formed from the Li atoms and *ipso*-oxygens of the phenol moieties.

With the exception of dimeric **Li3**, the dipp-substituted complexes generally displayed Li_4O_4 cubane structures (**Li1**, **Li5** and **Li7**) when crystallized from toluene solvent (Figures S57, S61-S63, refer to ESI for further details). Each tetracoordinate Li bonds to three phenolic oxygen atoms and a nitrogen atom from the imine group to give a distorted tetrahedral environment ($\tau_{4\text{-Li1}}$ = 0.65, $\tau_{4\text{-Li5}}$ = 0.64, $\tau_{4\text{-Li7}}$ = 0.65).[38] With **Li7**, a differ-

ent solvate was obtained when toluene was replaced by THF as the crystallization solvent, which decreased the aggregation state from a tetramer to a dimer (Figure 4). The fourth Li coordination site, originally occupied by a third phenolic oxygen, is instead satisfied with one equivalent of Lewis donor THF. This closely mirrors the structure of **Li2** (Figure S58), also crystallized from THF solvent, where the lithium atoms coordinate two phenolic oxygen atoms, one imine nitrogen and one THF oxygen to give a distorted tetrahedral coordination geometry ($\tau_{4\text{-Li2}} = 0.76$, $\tau_{4\text{-Li7}} = 0.75$). Replacing one Li–O-(phenoxyimine) bond with a Li–O(THF) bond reduces the constrained geometry around the Li center, as indicated by the increased τ_4 values.

In general, the C_{ipso}-O bond lengths of the lithium complexes are significantly shorter [1.296(2)–1.321(12) Å, Table S4] than the related protonated ligand bearing a naphthalene imine substituent [C–O, 1.354(2) Å].[41] These short C–O bonds suggest resonance delocalization of the anionic charge throughout the phenoxyimine ligand. Furthermore, the C–C bond lengths in the (O–)C=C–C(=N) scaffold of these complexes [1.447(3)–1.465(14) Å, Table S4] lie between the expected bond lengths for aromatic single and double bonds (1.52 and 1.40 Å, respectively),[42] indicating resonance delocalization with the imine group, which is further supported by the $LiNC_3O$ ring being placed almost coplanar to the phenol moiety ($\theta < 15°$). The resonance delocalization is similar for all of the complexes (Table S4), suggesting that the ligand substitution does not have a significant influence.

The study of the solution-state structure of organometallic complexes is a powerful approach to investigate the behavior in polymerization processes.[43] DOSY NMR spectroscopy is a useful tool to determine the aggregation state, and complexes **Li1**-**Li7** were thus characterized by DOSY analysis. The diffusion coefficients were compared to a calibration plot to determine a predicted molecular weight (refer to ESI for further details). Correlating with the overall trends observed for the solid-state structures, DOSY analysis indicated that all complexes were dimers in d_8-THF solution, except from **Li2** and **Li3**, which both feature sterically bulky *ortho*-^{t}Bu groups and give diffusion coefficients that lie intermediate between a monomer and a dimer and may indicate a rapid equilibrium between these two aggregation states. While the predicted molecular weight of **Li2** is closer to a dimer, **Li3** lies closer to a monomeric structure, attributed to the sterically bulky N-dipp substituents (*vs.* N–Me in **Li2**) reducing the aggregation state. In d_8-toluene, higher aggregation states were observed: **Li3** was dimeric, **Li2** was trimeric, **Li4** was tetrameric and **Li1**, **Li5** and **Li7** appear to undergo trimer/tetramer equilibria, which may suggest that these structures can undergo dynamic equilibria in solution.[44,45] **Li6** was insoluble in d_8-toluene, however it is important to note that this complex fully dissolves under the polymerization conditions (in THF solvent). The DOSY studies coupled with the X-ray diffraction studies highlight the differences in aggregation between the solid state and the solution state, yet the general trends are maintained and depend upon the ligand substituents. Notably, the aggregation state may influence the electronics of the Li center, as in d_8-toluene, the ^{7}Li NMR resonance of dimeric **Li3** ($\delta = 2.64$ ppm) is significantly deshielded compared to **Li1** ($\delta = 1.86$ ppm), **Li5** ($\delta = 2.16$ ppm) and **Li7** ($\delta = 1.61$ ppm). The accompanying ^{1}H NMR spectra also vary. Whilst *para*-chloro-substituted **Li7** displays two doublets for the dipp-CH_3 groups ($\delta = 0.87$ and 0.63 ppm), the *ortho*-chloro-substituted analogue **Li5** displays four doublets ($\delta =$ 1.11, 1.02, 0.70 and 0.41 ppm). This difference is attributed to the *ortho*-Cl blocking rotation of the dipp substituent, unlike the *para*-substituted analogue. While **Li3** bears a bulky *ortho*-^{t}Bu-substituent, the reduced aggregation state is proposed to enable free rotation of the dipp groups, resulting in only two resonances for the methyl groups ($\delta = 1.07$ and 1.01 ppm). With **Li7**, THF solvent decreased the solid-state aggregation from a tetramer to a dimer; in d_8-THF solution, only one ^{1}H signal was observed from the dipp-CH_3 groups (instead of the two observed in d_8-toluene solution), providing further support for THF coordination decreasing the solution-state aggregation.

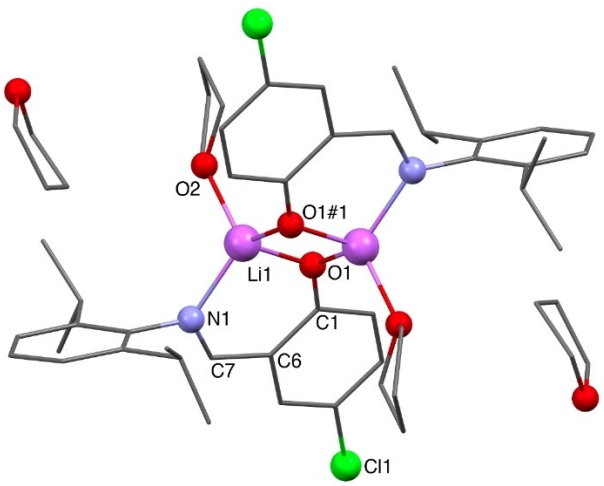

Figure 4. Molecular structure of **Li7**•THF crystallized from THF solvent. Hydrogen atoms have been omitted for clarity.

Polymerization studies

Lithium complexes **Li1**-**Li7** were investigated as potential initiators for the ROP of *rac*-LA. These reactions were performed at ambient temperature in THF solvent with a loading ratio of [LA]:[Li] = 100:1 in the presence of 1 eq. BnOH, which has been shown to be important in the initiation of *rac*-LA ROP with several different catalyst systems.[46,47] THF was selected as the solvent after optimization of the reaction conditions (Table 1, entries 9–12), as this Lewis base solvent not only improves the solubility of *rac*-LA but also reduces the catalyst aggregation state, which may enhance monomer accessibility to the metal center.[48–50] All lithium complexes except from **Li4** showed high catalytic activity ($k_{obs} \leq 7.43 \times 10^{-2}$ s^{-1}), giving almost complete conversion of *rac*-LA within 1 minute (Table 1). Kinetic studies show that the polymerizations with **Li1**-**Li3** and **Li5**-**Li7** were all first order in monomer (Figure 5). The excellent activities are

Table 1. Polymerization data for *rac*-LA with complexes **Li1**-**Li7**, **Na6**, **K6**.[a]

Entry	[Cat.]	Time [s]	Conv.[b] [%]	$M_{n,theo}$[c] [g mol^{-1}] (1 chain)	$M_{n,theo}$[c] [g mol^{-1}] (2 chains)	$M_{n,obs}$[d] [g mol^{-1}]	$Đ$[d]	P_r[b]
1	**Li1**	30	68	9860	4930	7450	1.94	–
2	**Li1**	35	75	10840	5420	7690	2.06	0.54
3	**Li2**	30	89	12870	6430	7490	1.94	0.48
4	**Li3**	30	83	11960	5980	17990	1.90	–
5	**Li3**	60	98	14120	7060	12860	1.82	0.47
6	**Li4**	600	12	1768	889	–	–	–
7	**Li5**	30	45	6440	3220	2920	1.73	0.49
8	**Li5**	70	93	13460	6730	7110	1.85	0.52
9[e]	**Li5**	3600	34	4750	2380	15110	3.27	–
10[f]	**Li5**	5400	8	1190	600	–	–	–
11[g]	**Li5**	360	92	13250	6630	23620	2.11	0.56
12[h]	**Li5**	40	85	1220	610	1030	1.49	0.48
13	**Li6**	30	46	6620	3310	3440	1.31	0.51
14	**Li6**	40	70	10020	4810	4600	1.64	–
15	**Li6**	70	96	13840	6920	5440	1.77	0.52
16[i]	**Li6**	80	64	18550	9280	12040	1.74	0.55
17[j]	**Li6**	200	42	30140	15070	16920	1.82	0.56
18	**Li7**	30	62	8860	4430	5580	1.76	–
19	**Li7**	50	78	11220	5610	7610	1.94	0.40
20	**Na6**	30	96	13800	6900	18570	2.24	0.51
21	**K6**	30	93	13320	6660	14990	2.34	0.48

[a] Polymerization conditions: [cat.]:[BnOH]:[*rac*-LA] = 1 : 1 : 100, [*rac*-LA] = 1 M in THF, ambient temperature. Reactions were duplicated. [b] Determined by ^{1}H NMR spectroscopy. [c] Calculated as ([*rac*-LA]/[catalyst]) × (%conversion/100) × MW of *rac*-LA. [d] Determined by SEC in THF solvent, universal calibration relative to polystyrene standards, M_n was calculated considering Mark-Houwink's corrections for M_n (M_n(calc) = 0.58*[M_n(SEC)]).[56] [e] The reaction was carried out in THF without BnOH. [f] The reaction was carried out in toluene without BnOH. [g] The reaction was carried out in toluene at 120 °C without BnOH. [h] The reaction was carried out in toluene at 120 °C with the loading ratio of [cat.]:[BnOH]:[*rac*-LA] = 1 : 10 : 100. [i] The reaction was carried out with the loading ratio of [cat.]:[BnOH]:[*rac*-LA] = 1 : 1 : 200. [j] The reaction was carried out with the loading ratio of [cat.]:[BnOH]:[*rac*-LA] = 1 : 1 : 500.

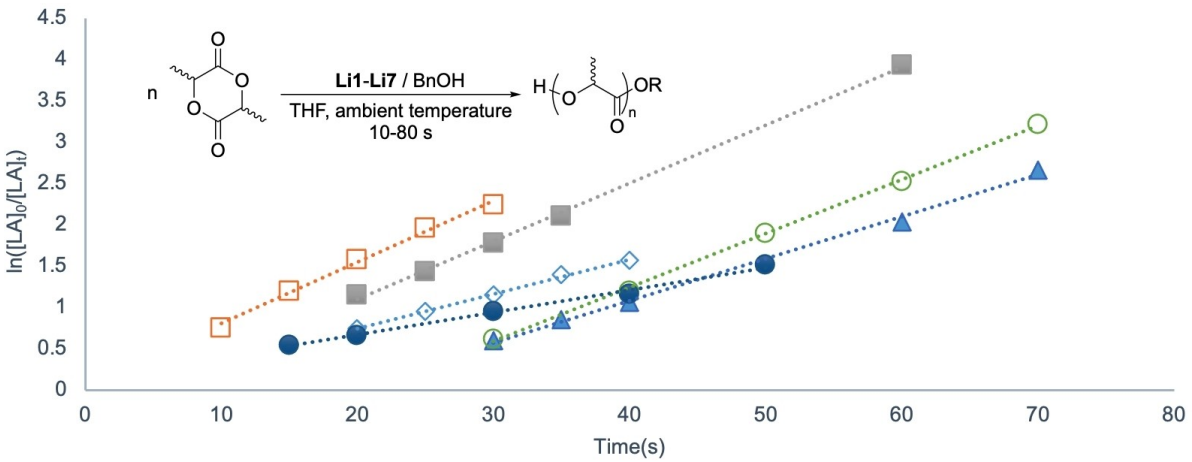

Figure 5. Semi-logarithmic plot of *rac*-LA conversion *vs.* time at room temperature with lithium complexes **Li1**-**Li7** in THF solvent with loading ratio of [cat.]:[BnOH]:[*rac*-LA] = 1 : 1 : 100: **Li1** ($k_{obs} = 4.21 \times 10^{-2}$ s^{-1}, $R^2 > 0.99$), **Li2** ($k_{obs} = 7.43 \times 10^{-2}$ s^{-1}, $R^2 = 0.99$), **Li3** ($k_{obs} = 7.04 \times 10^{-2}$ s^{-1}, $R^2 > 0.99$), **Li5** ($k_{obs} = 5.09 \times 10^{-2}$ s^{-1}, $R^2 > 0.99$), **Li6** ($k_{obs} = 6.53 \times 10^{-2}$ s^{-1}, $R^2 > 0.99$), **Li7**($k_{obs} = 2.70 \times 10^{-2}$ s^{-1}, $R^2 = 0.99$). **Li4** was also tested but displayed very low activity (giving only 12% conversion after 10 minutes; refer to Table S5 for further details).

attributed to the highly Lewis acidic lithium center facilitating monomer coordination hence activation towards nucleophilic attack and ring-opening.[4,23,51,52] The highest activities were observed for **Li2** ($k_{obs} = 7.43 \times 10^{-2}$ s^{-1}), closely followed by **Li3** ($k_{obs} = 7.04 \times 10^{-2}$ s^{-1}). This may at first appear counterintuitive, as both **Li2** and **Li3** bear bulky electron donating ^{t}Bu substituents, which are known to hinder monomer coordination both sterically (by blocking monomer access to the metal) and electronically (by reducing the metal Lewis acidity).[21] However, the steric bulk of the ^{t}Bu and dipp substituents reduces the aggregation state of **Li2** and **Li3** compared to the other complexes in d_8-THF solution (*vide supra*), likely increasing the accessibility of the metal center to facilitate monomer coordination. Bearing the bulky dipp substituent, **Li3** ($k_{obs} = 7.04 \times 10^{-2}$ s^{-1}) exhibits lower catalytic activity than **Li2** ($k_{obs} = 7.43 \times 10^{-2}$ s^{-1}), which suggests that both ligand sterics and the aggregation state influence the accessibility of the metal center and thus the polymerization activity.[45,53,54] To investigate

further, the catalytic activity of **Li6** was tested in the presence of tetramethylethylene diamine (TMEDA), a bidentate Lewis donor known to decrease the aggregation state of organolithium complexes (Table S6).[37,45,55] In the absence of BnOH, TMEDA significantly enhances the catalytic activity of **Li6**, increasing the conversion from 14% to 51% after 50 seconds. In addition to decreasing the aggregation state, coordination of the bidentate donor may increase the electron density at the metal center, thus increasing the nucleophilicity of the Li-alkoxide group to favor LA attack and ring-opening. However, in the presence of BnOH, TMEDA does not significantly influence the polymerization outcome; identical conversions of 70% were observed after 30 seconds. The limited influence of TMEDA in the presence of BnOH may arise because the Lewis donor alcohol can also decrease the catalyst aggregation state. Complexes **Li1** and **Li5**-**Li7** all display lower catalytic reactivity compared to **Li2** and **Li3**, which may be attributed to the increased aggregation state (Tables S1 and S2). In addition to influencing propagation rate, literature reports have suggested that catalyst aggregation can also influence initiation, by generating an induction period where the complex dissociates to form the active mononuclear species.[49] While a slight induction period is observed with **Li5**-**Li6**, this does not generally appear to be the case with these phenoxyimine Li complexes.

As the solid- and solution-state studies suggest that complexes **Li1** and **Li5**-**Li7** bear similar structural motifs in THF solvent (*vide supra*), this allows comparisons to be drawn independent of the aggregation state. Of these four complexes, there generally appears to be an inverse relationship between the catalytic activity and initiation efficiency (Figure 5). It could be expected that increasing the Lewis acidity of the metal center enhances the ability to coordinate LA but reduces the nucleophilicity of the metal-alkoxide towards ring-opening.[56] Of these four complexes, **Li6** gives the highest propagation rate ($k_{obs} = 6.53 \times 10^{-2}$ s^{-1}), with the longest induction period (21 seconds). This high activity is attributed to the *para*-chloro substituent increasing the Lewis acidity of the lithium center by inductively withdrawing electron density, without sterically blocking monomer coordination (compared to the *ortho*-substituted analogues **Li2**-**Li5**). The increased activity of **Li6** compared to the dipp-substituted analogue **Li7** is likely to arise from the reduced steric bulk facilitating LA access to the metal center. *Ortho*-chloro/N-dipp-substituted **Li5** shows catalytic activity, while N–Me-substituted **Li4** is almost inactive towards LA polymerization (Table 1, entry 6); this is tentatively attributed to the increased aggregation state of **Li4** both in the solid state (ladder structure) and the solution state (tetramer in d_8-toluene solvent) reducing the kinetic mobility of the catalyst species as well as decreasing the steric accessibility of the metal center. With structurally similar N-dipp-substituted **Li1**, **Li5** and **Li7**, complex **Li1** (unsubstituted phenol) gives a slower propagation rate than **Li5** (*ortho*-Cl) but is faster than **Li7** (*para*-Cl; **Li5** > **Li1** > **Li7**). This reactivity trend correlates to the ^{7}Li NMR shifts, where downfield chemical shifts may indicate an increased Lewis acidity of the lithium center and thus higher catalytic activity [**Li5**, $\delta = 1.45$ ppm; **Li1**, $\delta = 1.26$ ppm; **Li7**, $\delta = 1.07$ ppm in d_8-THF solvent]. However, other complexes including N-dipp-substituted **Li3** ($\delta = 1.29$ ppm) do not fit this trend, which implies that the catalytic activity is dependent on both the accessibility and the Lewis acidity of the metal center.

Inspection of the catalyst bond lengths and angles (Table S4) indicates that there is some correlation between the Li–N bond length and the catalytic activity, with longer Li–N bonds generally giving higher propagation rates for structurally similar complexes. With N-dipp-substituted complexes **Li1**, **Li5** and **Li7**, complex **Li5** displays the longest Li–N bond [2.096(3) Å] and the highest activity ($k_{obs} = 5.09 \times 10^{-2}$ s^{-1}), followed by **Li1** [Li–N = 2.024(4) Å, $k_{obs} = 4.21 \times 10^{-2}$ s^{-1}] and the least active complex **Li7** [Li-N = 1.99(2) Å, $k_{obs} = 2.70 \times 10^{-2}$ s^{-1}]. Longer and weaker Li–N dative bonds may enhance the catalytic activity through two separate mechanisms: firstly, through creating more space around the metal center thus facilitating LA coordination; secondly, by reducing the strength of the dative interaction and so increasing the Lewis acidity of Li.

Catalyst **Li6** tolerated an increased LA:catalyst ratio of 200:1 or 500:1 (where the catalyst is a 1:1 combination of **Li6** and BnOH, Table 1, entries 14, 16 and 17). Polymer characterization data suggests that the lithium complex can initiate the polymerization in the absence and presence of BnOH (Figures S70 and S71). This hypothesis is supported by size exclusion chromatography (SEC) and MALDI-ToF data, which shows both BnO/H end groups and cyclic polymer (refer to Polymerization mechanism studies, *vide infra*). *Ortho*-^{t}Bu substituted complex **Li3** is a notable exception, where the M_n values give better agreement with only one polymer chain being initiated per catalyst system. This may suggest that a different initiation mechanism occurs with **Li3** compared to the other complexes (*vide infra*). While complexes **Li1**-**Li7** display excellent catalyst activities, SEC analysis suggests that the polymerization is not particularly well controlled. In the presence of BnOH, the dispersities obtained were between 1.31 and 2.06 (Table 1), and generally increase as the polymerization progresses, which is attributed to transesterification reactions becoming competitive with propagation reactions in the late stages of the polymerization.[4] Accordingly, MALDI-ToF analysis of the polymers showed a repeat unit of $\triangle$ (m/z) = 72 g mol^{-1} and a mixture of cyclic polymers and linear α-benzoxy, ω-hydroxy end-capped polymers (Figure S67). The polymers were generally atactic, with P_r values ranging between 0.40 and 0.56 (Table 1), which is attributed to the extremely fast propagation rate although it should be noted that the achiral catalyst structures also disfavor stereocontrol from occurring through an enantiomorphic site control mechanism.[21]

Sodium and potassium analogues of **Li6** (**Na6** and **K6**) were also examined for the ROP of *rac*-LA to allow a comparison between different metal centers. Both metals showed a significantly higher catalytic activity compared to the lithium analogues; while **Li6** gave 46% conversion in 30 seconds, **Na6** and **K6** were twice as active, giving 96% and 93% conversion respectively (Table 1, entries 20–21). This enhanced activity can be ascribed to the increased ionic radius of sodium and potassium providing additional coordination sites for LA, as reported by Tabernero, Cano and colleagues.[34] Whilst the

catalytic activities are significantly higher, the polymerization control is reduced, giving broader dispersities. After 30 seconds, the dispersity achieved with **Li6** was 1.31, compared to **Na6** ($Đ = 2.24$) and **K6** ($Đ = 2.34$).

Complexes **Li3**, **Li5** and **Li6** were also investigated as initiators for *rac*-LA ROP without BnOH (Table 2), and were all significantly less active than in the presence of BnOH. Notably, when using **Li5** and **Li6** without BnOH, the $M_{n,obs}$ values suggest only one chain was initiated per catalyst, and the values were much higher than those obtained in the presence of BnOH, where the $M_{n,obs}$ values lie closer to two chains per catalyst (Table 2, entries 3–6). These control studies suggest that the phenoxyimine lithium complexes can initiate *rac*-LA ROP in the absence of a co-initiator. With **Li5**, the $M_{n,obs}$ value is significantly higher than $M_{n,theo}$ for one chain initiated per catalyst (entry 3), suggesting that not all of the catalyst may be activated. The dispersities for **Li5** and **Li6** were much broader in the absence of BnOH, which is attributed to inefficient initiation.[58] In contrast, the $M_{n,obs}$ value of **Li3** gave better agreement with one chain per catalyst in both the absence and the presence of BnOH (entries 1 and 2). This difference (*vs.* **Li5** and **Li6**) may arise from the co-initiator BnOH acting as a Lewis donor and decreasing the aggregation state of **Li5** and **Li6**, whereas **Li3** is already a monomer in the solution state (*vide supra*). Providing some support for this observation, the induction period of **Li3**/BnOH in the presence of BnOH is shorter than **Li5**/BnOH and **Li6**/BnOH (Figure 5). Notably, **Li3** gave much lower dispersity without BnOH. This trend differs from **Li5** and **Li6**, perhaps suggesting that the initiation mechanism differs. MALDI-ToF analysis of the polymers showed only cyclic polymers when the ratio of **Li5**:LA employed during the reaction was 1:100 in the absence of BnOH (Figure S69). However, when the **Li5**:LA ratio was decreased to 1:1, some ligand-end capped linear oligomers were observed in the MALDI-ToF spectrum (Figure S75). This observation indicated that intramolecular transesterification to form cyclic polymers is more prevalent in the late stages of the reaction, which may explain the decreased M_n values observed at high conversions (Table S5).

Polymerization mechanism studies

While ROP with half-salen complexes is often proposed to follow a coordination-insertion mechanism with non-alkali metals,[34,59] our results suggest that the initiation pathway may differ depending on the absence or presence of BnOH (in line with previous studies on alkali metal complexes).[34,52,60] Understanding the operative mechanism in these (and related alkali metal) catalysts is important in order to identify opportunities to improve catalyst activity and control. Indeed, previous studies have shown that external alcohols can play multiple roles, by reacting with an organometallic precursor to form an active metal-alkoxide initiator, directly initiating the polymerization through an activated monomer mechanism (Scheme 1, right), and/or by acting as a chain transfer agent under immortal polymerization conditions.[60] The stoichiometric reaction of **Li5** and *rac*-LA was thus investigated by NMR spectroscopy (d_8-THF solvent, ambient temperature, Scheme S1). A broad resonance was observed at 5.14 ppm in the ^{1}H NMR spectrum, with a small upfield shift (0.04 ppm) compared to free LA (Figure S73). The ^{7}Li NMR spectrum (Figure S74) shows there are two lithium environments: one is **Li5** ($\delta_{Li5} = 1.45$ ppm) and the other is shifted upfield ($\delta = 0.72$ ppm). To ascertain whether these differences were caused by monomer coordination or LA ring-opening, NMR studies were performed with γ-valerolactone (γ-VL), a cyclic ester which is challenging to polymerize. The resultant ^{7}Li NMR spectrum gave a resonance at $\delta = 0.66$ ppm, which was attributed to Lewis acid/base co-complexation between γ-VL and **Li5**. The similarity between this ^{7}Li NMR resonance and that of **Li5** with LA ($\Delta\delta = 0.06$ ppm) may suggest that **Li5** and LA interact through Lewis acid/base coordination rather than ring-opening. However, MALDI-ToF analysis of the reaction product showed a mixture of cyclic and ligand-end capped oligomeric PLA (Figure S75), suggesting that **Li5** can initiate LA ROP. This observation was further supported by DOSY spectroscopy, where **Li5** and ring-opened *rac*-LA resonances were observed at the same diffusion coefficient, unlike non-coordinated LA (Figure S76). Through comparison to a calibration plot, the observed MW of the mixture of **Li5** and LA is 703 g mol^{-1}, which is significantly higher than that of **Li5** alone (565 g mol^{-1}, refer to Table S1), suggesting that LA interacts with dinuclear **Li5** (Scheme 3A). Taken together, these observations suggest that in the absence

Table 2. Polymerization data for *rac*-LA with lithium complexes **Li3**, **Li5** and **Li6** with and without BnOH.[a]

Entry	[Cat.]	[Cat.]:[LA]:[BnOH]	Time [s]	Conv.[b] [%]	$M_{n,theo}$[c] [g mol^{-1}] (1 chain)	$M_{n,theo}$[c] [g mol^{-1}] (2 chains)	$M_{n,obs}$[d] [g mol^{-1}]	$Đ$[d]
1	**Li3**	1:100:0	900	86	12450	6220	9690	1.01
2[e]	**Li3**	1:100:1	35	88	12650	6320	15240	1.96
3	**Li5**	1:100:0	3600	33	4750	2430	15110	3.27
4	**Li5**	1:100:1	70	93	13460	6730	7110	1.85
5	**Li6**	1:100:0	900	88	12670	6340	12660	3.41
6[f]	**Li6**	1:100:1	70	96	13840	6920	5800	1.71

[a] Polymerization conditions: [*rac*-LA] = 1 M in THF; room temperature. Reactions were duplicated. [b] Determined by ^{1}H NMR spectroscopy. [c] Calculated as ([*rac*-LA] / [catalyst]) × (%conversion/100) × MW of *rac*-LA. [d] Determined by size exclusion chromatography (SEC) in THF solvent, universal calibration relative to polystyrene standards, M_n was calculated considering Mark-Houwink's corrections for M_n (M_n(calc) = 0.58*[M_n(SEC)]).[56] [e] $P_r = 0.46$, determined by ^{1}H NMR spectroscopy (refer to ESI for details). [f] $P_r = 0.54$.

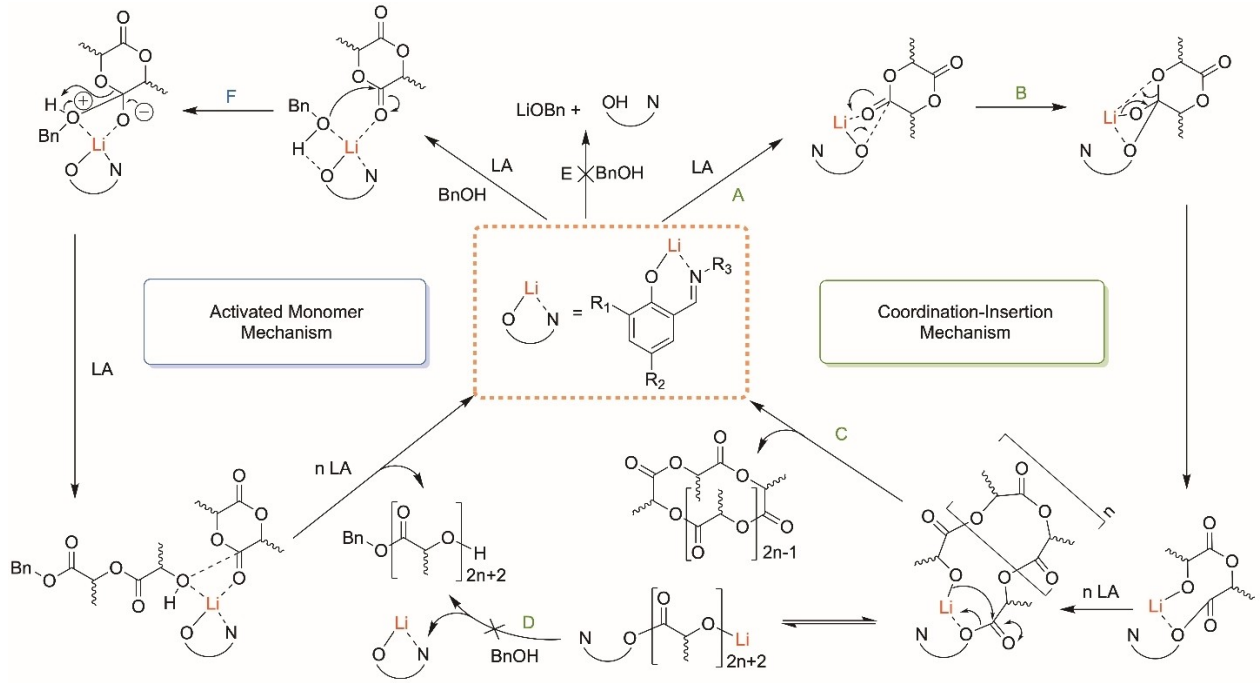

Scheme 3. Proposed mechanism for ROP of *rac*-LA initiated by half-salen lithium complexes in the presence and absence of co-initiator BnOH.

of BnOH, the mechanism is likely to occur through a coordination-insertion mechanism (Scheme 3, right), initiated by insertion of LA into the Li-phenolate bond. The predominance of cyclic esters formed in the absence of BnOH (determined by MALDI-ToF analysis, Figures S69 and S75) provides further support for this initiation route (Scheme 3B), as intramolecular transesterification to form cyclic PLA (Scheme 3C) would regenerate the **Li5** catalyst, which bears a more stable phenolate anion (*vs.* the propagating Li-alkoxide polymer chain). Increasing the **Li5**:LA ratio from 1:1 to 1:10 generated cyclic oligomers of increased molecular weight, according to DOSY analysis (Figures S76 and S77). However, **Li5** was observed in the ^{1}H NMR spectra for each of these reactions, which indicates that while catalyst **Li5** can perform the initiation, not all of the catalyst species is active and thus the initiation is likely to be inefficient. A stoichiometric reaction of **Li3** and *rac*-LA in a ratio of 1:1 was also investigated by NMR spectroscopy (d_8-THF solvent, ambient temperature) and gave LA conversion of 18% after 24 h (Figure S78).

Next, BnOH (1 eq.) was added to the stoichiometric reaction between **Li5** (1 eq.) and *rac*-LA (1 eq., d_8-THF, ambient temperature, overnight reaction), which almost immediately increased the LA conversion from 39% to 90%. This observation emphasizes that BnOH dramatically increases the polymerization rate. Here, MALDI-ToF analysis only showed α-benzoxy, ω-hydroxy end-capped linear polymers and cyclic polymers. No ligand end-capped linear polymers were observed; this could arise from transesterification reactions between BnOH and ligand-end capped PLA. To investigate this possibility, the reaction between **Li5**, BnOH and PLA (prepared using **Li5** only) in a ratio of 1:1:100 (PLA mass based on 100 *rac*-LA units) was investigated under polymerization conditions (THF, ambient temperature, Scheme S2). No benzoxide-end groups were observed in the MALDI-ToF analysis, suggesting no reaction occurs between BnOH and ligand-end capped PLA (Scheme 3D, Figure S79). Instead, BnOH could react with **Li5** to produce LiOBn, yet ^{1}H NMR spectroscopic analysis and DOSY studies of the stoichiometric reactions between lithium complexes (**Li5** or **Li3**) and BnOH (d_8-THF, Scheme 3E, Figures S80 and S81) shows that no reaction occurs, which can be attributed to the greater acidity of the half-salen ligand *vs.* BnOH. This was further confirmed by the reaction of LiOBn and ligand **L5** in a 1:1 ratio, which reacted completely and produced **Li5** and BnOH in a 1:1 ratio. These observations suggest that the new polymers generated after BnOH addition were only derived from the activated monomer (BnOH initiated) polymerization of the unreacted LA, with cyclic PLA formed prior to BnOH addition. The stoichiometric reaction between BnOH and **Li4** was also investigated and neither reaction nor BnOH/Li coordination was observed by ^{1}H NMR analysis (d_8-THF, Figure S82), although BnOH coordination may occur in dynamic equilibrium with d_8-THF coordination.

Finally, the stoichiometric reaction between **Li5**, LA and BnOH was investigated by NMR spectroscopy under the same reaction conditions (d_8-THF, ambient temperature, Scheme S4), which showed the presence of LA, PLA and unreacted **Li5**, giving an almost identical ^{1}H and ^{7}Li NMR spectra to the equivalent reaction with BnOH added later (Figures S74 and S83). It is therefore likely that, in the presence of BnOH, the reaction proceeds through an activated monomer mechanism (Scheme 3, left), rather than a coordination-insertion mechanism as claimed for some related phenolate-alcohol systems

(Scheme 3, right). All three species (**Li5**, LA and BnOH) may interact in solution to activate BnOH through N···H or $O_{phenolate}$···H hydrogen bonding, as has been reported for other ROP catalyst systems (Scheme 3F), however our DOSY studies did not provide definitive proof for this interaction (Figure S84).[46,52] These results highlight the importance of considering the complex dynamic equilibria which can exist in solution. As a result of these dynamic equilibria and different aggregation states, it is likely that different reactivity pathways including both coordination-insertion and activated monomer mechanisms could occur simultaneously in solution.

Conclusions

Seven lithium complexes supported by half-salen ligands have been prepared and characterized. The molecular structure of complexes **Li1**-**Li5** and **Li7** were confirmed by single crystal X-ray diffraction techniques. In the solid-state, these complexes show dinuclear, tetranuclear or polymeric structures depending on the ligand substituent(s) and bulk solvent, with complex **Li4** representing the first lithium-phenoxyimine "ladder" structure. Detailed DOSY NMR studies suggest that in solution, dynamic equilibria occur between different aggregation states; the aggregation state depends on the ligand substituents and influences the electronics of the Li center. While the aggregation states differ between the solid- and solution-state structures, the general trends are maintained and influence catalyst performance, which is linked to the kinetic mobility and metal accessibility. Complexes **Li1**-**Li7** generally displayed excellent activities toward ROP of *rac*-LA in the presence of BnOH ($k_{obs} \leq 7.43 \times 10^{-2}\ s^{-1}$), albeit with moderate control. The polymerization activity strongly depends on the aggregation state, increasing for catalysts with lower aggregation in the solid-state (**Li3**, dimer, $k_{obs} = 7.04 \times 10^{-2}\ s^{-1}$; **Li5**, tetramer, $k_{obs} = 5.09 \times 10^{-2}\ s^{-1}$; **Li4**, polymeric ladder, inactive). Na and K complexes revealed faster catalyst activity than Li complexes (although with poorer control), providing further evidence that metal accessibility can enhance the catalyst activity. Small molecule reactivity studies combined with kinetic investigations indicate that both catalyst and co-initiator BnOH can initiate polymerization through different mechanisms. To some extent, BnOH can be utilized to switch between the two catalytic mechanisms. In the absence of BnOH, the polymerization proceeds through a coordination-insertion mechanism whereas an activated monomer mechanism operates in the presence of BnOH. However, dynamic equilibria of different aggregation states and lithium species can occur in solution, and thus both mechanisms may act simultaneously when BnOH is used as a co-initiator. This study highlights the importance of understanding the equilibria that can occur between different species in solution, in order to develop active and controlled catalysts for the ROP of *rac*-LA.

Experimental Section

General experimental

All manipulations involving air- or moisture-sensitive compounds were performed under argon atmosphere using standard Schlenk-line techniques and gloveboxes. All reagents were purchased from Sigma-Aldrich, Fisher Scientific Honeywell and Fluorochem Ltd. and used as received unless stated otherwise. Dry solvents (hexane, THF and toluene) were collected from a solvent purification system and stored in the presence of activated molecular sieves (4 Å) under an argon atmosphere. Deuterated solvents (d_8-toluene and d_8-THF) were degassed by three freeze-pump-thaw cycles and stored in a glovebox in the presence of activated 4 Å molecular sieves. Standardization of organolithium reagent ^{n}BuLi was performed by titration with (−)-menthol and 1, 10-phenanthroline. *Rac*-lactide was purified by double recrystallization from toluene followed by sublimation under vacuum and was subsequently stored in the glove box freezer at −34 °C. Benzyl alcohol (BnOH) and valerolactone (γ-VL) was dried over CaH_2 and distilled under reduced pressure prior to use.

1D (^{1}H, ^{13}C and ^{7}Li) NMR spectra were recorded with a Bruker AVA500 or PRO500 spectrometer at ambient temperature with the chemical shifts referenced to residual solvent resonances. The chemical shifts (δ) are quoted relative to tetramethylsilane. Spectra were assigned using correlation between hydrogen atoms and carbon atoms identified through ^{1}H-^{1}H COSY (Correlation Spectroscopy) and ^{1}H-^{13}C HSQC (Heteronuclear Single Quantum Correlation) NMR spectroscopic methods. Diffusion-Ordered Spectroscopy (DOSY) NMR experiments were obtained using a Bruker AVA500 spectrometer. The DOSY plot was generated using the DOSY processing module of TopSpin. Parameters were optimized empirically to find the best quality of data for explanation purposes. Elemental microanalysis was performed by Stephen Boyer at London Metropolitan University and Elemental Microanalysis Ltd. Molecular weights of polymers were determined by size exclusion chromatography (SEC) in a 1260 Infinity II SEC single detection system with mixed bed C PLgel columns (300 × 7.5 mm) and were calibrated using polystyrene standards and corrected by a Mark-Houwink factor of 0.58.[57] Mass spectrometry (MS) data for ligands was carried out using accurate electrospray ionization MS in the positive ion mode and collected on a Thermo Fisher Scientific TRACE™ GC Ultra gas chromatograph. MALDI-ToF mass analysis was performed using a Bruker Daltonics UltrafleXtreme™ MALDI-ToF/ToF MS instrument. Dithranol was used as matrix and potassium iodide was added as a cationising additive. Melting points were measured in triplicate on a Mel-Temp apparatus and were uncorrected.

Synthesis and characterization of phenoxyimine ligands (general protocol) L1-L7

Seven half-salen ligands (**L1**-**L7**) were synthesized based on an adapted literature procedure.[33,61,62] Dependent on the ligand, a solution of amine (methylamine or 2,6-diisopropylaniline, 2 mmol) in ethanol (5 mL) was added dropwise to a solution of salicylaldehyde (salicylaldehyde, 3-*tert*-butylsalicylaldehyde, 3-chlorosalicylaldehyde or 5-chlorosalicylaldehyde, 2 mmol) in ethanol (5 mL). The resulting yellow solutions were stirred and refluxed for 3 hours in the presence of acetic acid as a catalyst, and the solvent was subsequently removed *in vacuo*. Ligands **L1**-**L7** were purified through recrystallization from ethanol to produce yellow crystals.

Ligand **L1**: (547 mg, 97.1 %). M.p. 60–63 °C. ^{1}H NMR (500 MHz, $CDCl_3$): δ 13.08 (s, 1H, OH), 8.31 (s, 1H, N=CH), 7.43 (t, 1H, J = 8.7, ArH), 7.36 (d, 1H, J = 7.7, ArH), 7.20 (m, 3H, ArH), 7.08 (d, J = 8.4, 1H,

ArH), 6.98 (t, 1H, J = 7.6, ArH), 3.01 (hept, 2H, J = 6.8, CH), 1.19 (d, 12H, J = 6.9, CH_3). ^{13}C NMR (126 MHz, $CDCl_3$): δ 166.8 (C=N), 161.4 (C–OH), 146.3 (C–N), 138.9, 133.4, 132.4, 125.6, 123.4, 119.2, 118.8, 117.5 (Ar–C), 28.28 (CH), 23.78 (CH_3). Both spectra gave good agreement with literature reports.[63] ESI-MS: *m/z* $[M]^+$: 281.19 calculated $[M]^+$: 281.18.

Ligand **L2**: (370 mg, 98.4 %) M.p. 30–31 °C. ^{1}H NMR (500 MHz, $CDCl_3$): δ 14.12 (s, 1H, OH), 8.35 (s, 1H, N=CH), 7.32 (d, 1H, J = 7.8, ArH), 7.10 (d, 1H, J = 7.6, ArH), 6.81 (t, 1H, J = 7.7, ArH), 3.48 (s, 3H, N–CH_3), 1.45 (s, 9H, C–CH_3). ^{13}C NMR (126 MHz, $CDCl_3$): δ 167.1 (C=N), 160.7 (C-OH), 137.7 (C–N), 129.5, 129.4, 118.9, 117.8 (Ar–C), 45.77 (N–CH_3), 34.98 (CCH_3), 29.47 (CCH_3). Elemental Analysis Calculated for $C_{19}H_{23}NO$ (191.27 g mol^{-1}): C 75.35, H 8.96, N 7.32. Found: C 74.35, H 8.87, N 7.28. ESI-MS: *m/z* $[M]^+$: 191.13 calculated$[M]^+$: 191.13.

Ligand **L3**: (532 mg, 78.9 %) M.p. 67–69 °C. ^{1}H NMR (500 MHz, $CDCl_3$): δ 13.61 (s, 1H, OH), 8.32 (s, 1H, N=CH), 7.45 (d, 1H, J = 7.8, ArH), 7.23 (d, 1H, J = 7.6, ArH), 7.19 (m, 3H, ArH), 6.92 (t, 1H, J = 7.6, ArH), 3.04 (hept, 2H, J = 6.9, CH), 1.52 (s, 9H, CH_3), 1.21 (d, 12H, J = 6.9, CH_3). ^{13}C NMR (126 MHz, $CDCl_3$): δ 167.7 (C=N), 160.8 (C-OH), 146.4, 139.0, 138.0, 130.7, 130.5, 125.5, 123.4, 118.7, 118.3 (Ar–C), 35.13 (CH), 29.56 (CH_3), 28.25 (CH), 23.75 (CH_3). Both spectra gave good agreement with literature reports.[64] ESI-MS: *m/z* $[M]^+$: 337.25 calculated$[M]^+$: 337.24.

Ligand **L4**: (533 mg, 98.2 %) M.p. 84–86 °C. ^{1}H NMR (500 MHz, $CDCl_3$): δ 14.50 (s, 1H, OH), 8.30 (d, 1H, J = 1.4, N=CH), 7.40 (dd, 1H, J = 7.9, 1.6, ArH), 7.14 (dd, 1H, J = 7.7, 1.6, ArH), 6.77 (t, 1H, J = 7.8, ArH), 3.50 (d, 3H, J = 1.5, CH_3). ^{13}C NMR (126 MHz, $CDCl_3$): δ 165.8 (C=N), 158.7 (C–OH), 132.7, 129.6, 122.3, 119.4, 118.2 (Ar–C), 45.0 (CH_3). Both spectra gave good agreement with literature reports.[61] EI-MS: *m/z* $[M]^+$: 169.02 calculated $[M]^+$: 169.03.

Ligand **L5**: (628 mg, 99.4 %) M.p. 104–108 °C. ^{1}H NMR (500 MHz, $CDCl_3$): δ 13.94 (s, 1H, OH), 8.30 (s, 1H, N=CH), 7.52 (d, 1H, J = 7.9, ArH), 7.29 (d, 1H, J = 7.7, ArH), 7.20 (s, 3H, ArH), 6.93 (t, 1H, J = 7.8, ArH), 2.98 (hept, 2H, J = 6.89, CH), 1.18 (d, 12H, J = 6.9, CH_3). ^{13}C NMR (126 MHz, $CDCl_3$): δ 166.3 (C=N), 157.3 (C–OH), 145.6, 139.0, 133.6, 130.8, 126.0, 123.5, 122.1, 119.7, 119.4 (Ar–C), 28.3 (CH), 23.71 (CH_3). Elemental Analysis Calculated for $C_{19}H_{22}ClNO$ (315.84 g mol^{-1}): C 72.25, H 7.02, N 4.43. Found: C 72.19, H 7.06, N 4.44. ESI-MS: *m/z* $[M]^+$:315.14 calculated$[M]^+$: 315.14.

Ligand **L6**: (322 mg, 95.0 %) M.p. 61–62 °C. ^{1}H NMR (500 MHz, $CDCl_3$): δ 13.30 (s, 1H, OH), 8.27 (s, 1H, N=CH), 7.23 (dd, 1H, J = 8.7, ArH), 7.21 (d, 1H, J = 2.6, ArH), 6.90 (d, 1H, J = 8.7, ArH), 3.50 (d, 3H, J = 1.5, CH_3). ^{13}C NMR (126 MHz, $CDCl_3$): δ 165.2 (C=N), 160.0 (C–OH), 132.1, 130.3 (Ar–C), 123.1 (C–Cl), 119.7, 118.8 (Ar–C), 46.11 (CH_3). Elemental Analysis Calculated for C_8H_8ClNO (169.61 g mol^{-1}): C 56.65, H 4.75, N 8.26. Found: C 56.31, H 4.70, N 8.16. EI-MS: *m/z* $[M]^+$: 168.96 calculated $[M]^+$: 169.03.

Ligand **L7**: (604 mg, 95.6 %) M.p. 114–115 °C. ^{1}H NMR (500 MHz, $CDCl_3$): δ 13.08 (s, 1H, OH), 8.24 (s, 1H, N=CH), 7.35 (d, 1H, J = 8.8, ArH), 7.32 (d, 1H, J = 2.6, ArH), 7.19 (s, 3H, ArH), 7.01 (d, 1H, J = 8.8, ArH), 2.95 (hept, 2H, J = 6.9, CH), 1.18 (d, 12H, J = 6.9, CH_3). ^{13}C NMR (126 MHz, $CDCl_3$): δ 165.6 (C=N), 159.9 (C–OH), 145.9, 138.7, 133.2, 131.4, 125.9, 123.9, 123.5, 119.5, 119.1 (Ar–C), 28.32 (CH), 23.67 (CH_3). Elemental Analysis Calculated for $C_{19}H_{22}NO$ (315.84 g mol^{-1}): C 72.25, H 7.02, N 4.43. Found: C 72.15, H 7.06, N 4.42. EI-MS: *m/z* $[M]^+$:315.15 calculated$[M]^+$: 315.14.

Synthesis and characterization of (phenoxyimine)Li complexes Li1-Li7

The lithium half-salen complexes were prepared according to a modified literature procedure.[35] In a glove box, the half-salen ligand, either **L1** (0.2814 g, 1 mmol), **L2** (0.1913 g, 1 mmol), **L3** (0.3375 g, 1 mmol), **L4** (0.1696 g, 1 mmol), **L5** (0.3158 g, 1 mmol), **L6** (0.1696 g, 1 mmol) or **L7** (0.3159 g, 1 mmol), was added to a Schlenk flask and dissolved in dry hexane (3 mL). ^{n}BuLi (1.6 M in hexane, 0.625 mL, 1 mmol) for ligands **L1**, **L3**, **L5** and **L6**, or a solution of Li[N{Si(CH_3)$_3$}$_2$] (0.1673 g, 1 mmol) in dry hexane (3 mL) for ligands **L3**, **L4** and **L7**, was then added dropwise and the resulting mixture was stirred for 3 hours at ambient temperature. The solvent was subsequently removed *in vacuo*. Complexes **Li1**-**Li7** were obtained as pale-yellow powders. Complexes **Li1**, **Li3**-**Li5** and **Li7** were crystallized from toluene, complexes **Li1**, **Li2** and **Li7** were crystallized from THF at −34 °C.

Complex **Li1**: (224 mg, 85.0 %) ^{1}H NMR (500 MHz, d_8-toluene): δ 7.84 (s, 1H, N=CH), 7.04-7.00 (m, 3H, dipp-ArH), 6.89 (dd, J = 7.7, 1.9 Hz, 1H, ArH), 6.81 (ddd, J = 8.8, 6.1, 1.9 Hz, 1H, ArH), 6.68 (dd, J = 8.3, 1.2 Hz, 1H, ArH), 6.44 (td, J = 7.4, 1.1 Hz, 1H, ArH), 2.64 (hept, J = 6.8 Hz, 2H, dipp-CH), 0.96 (d, J = 6.8 Hz, 6H, dipp-CH_3), 0.63 (d, J = 6.8 Hz, 6H, dipp-CH_3). ^{13}C NMR (126 MHz, d_8-toluene): δ 170.9 (C=N), 168.7 (C–O), 150.6 (C–N), 139.4 (dipp–Ar), 136.9, 135.0(Ar–C), 124.7, 123.4 (dipp–Ar), 122.4, 122.3, 115.6 (Ar–C), 28.7 (CH), 25.7, 22.2 (CH_3). ^{7}Li NMR (194 MHz, d_8-toluene): δ 1.86. Elemental Analysis Calculated for [{**Li1**}$^•$THF, $C_{23}H_{30}LiNO_2$] (359.44 g mol^{-1}): C 76.86, H 8.41, N 3.90. Found: C 76.60, H 8.50, N 3.90. MALDI-ToF-MS: *m/z* $[M+H]^+$: 288.21 calculated $[M+H]^+$: 288.19.

Complex **Li2**: (140 mg, 71.9 %) ^{1}H NMR (500 MHz, d_8-toluene): δ 7.60 (s, 1H, N=CH), 7.38 (dd, J = 7.6, 2.1 Hz, 1H, ArH), 6.92 (dd, J = 7.6, 2.0 Hz, 1H, ArH), 6.66 (t, J = 7.6 Hz, 1H, ArH), 2.30 (d, J = 1.4 Hz, 3H, CH_3), 1.40 (s, 9H, CCH_3). ^{13}C NMR (126 MHz, d_8-toluene): δ 169.9 (C=N), 166.2 (C–O), 140.3, 136.0, 130.7, 125.9, 114.6 (Ar–C), 46.6 (CH_3), 34.9 (CCH_3), 31.1 (CCH_3). ^{7}Li NMR (194 MHz, d_8-toluene): δ 2.03. Elemental Analysis Calculated for [{**Li2**}$^•$(THF)$_{0.5}$, $C_{14}H_{20}LiNO_{1.5}$] (233.26 g mol^{-1}): C 72.09, H 8.64, N 6.00. Found: C 71.95, H 8.72, N 6.09. MALDI-ToF-MS: *m/z* $[M+H]^+$: 198.11 calculated $[M+H]^+$: 198.14.

Complex **Li3**: (251 mg, 73.2 %) ^{1}H NMR (500 MHz, d_8-toluene): δ 8.05 (s, 1H, N=CH), 7.30 (dd, J = 7.6, 1.9 Hz, 1H, ArH), 7.08-6.99 (m, 3H, dipp-ArH), 7.00 (dd, 1H, ArH), 6.59 (t, J = 7.6 Hz, 1H, ArH), 2.98 (hept, J = 6.9 Hz, 2H, dipp-CH), 1.27 (s, 9H, C(CH_3)), 1.04 (dd, J = 30.1, 6.9 Hz, 12H, dipp-CH_3). ^{13}C NMR (126 MHz, d_8-toluene): δ 171.9 (C=N), 168.2 (C–O), 149.4 (C–N), 139.8 (Ar–C), 139.7 (dipp–Ar), 135.6, 131.7(Ar–C), 125.7, 123.6(dipp–Ar), 123.2, 114.2 (Ar–C), 34.42 (CCH_3), 30.36 (CCH_3), 28.56 (dipp-CH), 25.08, 22.81 (dipp-CH_3). ^{7}Li NMR (194 MHz, d_8-toluene): δ 2.64. Elemental Analysis Calculated for $C_{23}H_{30}LiNO$ (343.44 g mol^{-1}): C 80.44, H 8.81, N 4.08. Found: C 79.85, H 8.79, N 4.08. MALDI-ToF-MS: *m/z* [$[M+H]^+$: 344.29 calculated $[M+H]^+$: 344.25.

Complex **Li4**: (154 mg, 87.6 %) ^{1}H NMR (500 MHz, d_8-toluene): δ 7.68 (s, 1H, N=CH), 7.30 (d, J = 8.1 Hz, 1H, ArH), 6.81 (d, J = 7.9 Hz, 1H, ArH), 6.38 (t, J = 7.6 Hz, 1H, ArH), 2.88 (s, 3H, CH_3). ^{13}C NMR (126 MHz, d_8-toluene): δ 167.2 (C=N), 162.4 (C–O), 134.1, 131.3, 126.4, 125.6, 113.9 (Ar–C), 48.03 (CH_3). ^{7}Li NMR (194 MHz, d_8-toluene): δ 1.80. Elemental Analysis Calculated for $C_8H_7ClLiNO$ (175.54 g mol^{-1}): C 54.74, H 4.02, N 7.98. Found: C 54.53, H 3.93, N 7.72. MALDI-ToF-MS: *m/z* $[M+H]^+$: 176.02 calculated $[M+H]^+$: 176.04.

Complex **Li5**: (172 mg, 53.5 %) ^{1}H NMR (500 MHz, d_8-toluene): δ 7.87 (d, J = 1.5 Hz, 1H, N=CH), 7.08-6.99 (m, 3H, dipp-ArH), 6.90 (dd, J = 7.7, 1.8 Hz, 1H, ArH), 6.77 (dd, J = 7.9, 1.8 Hz, 1H, ArH), 6.24 (t, J = 7.7 Hz, 1H, ArH), 2.96 (hept, J = 6.7 Hz, 1H, dipp-CH), 2.41 (hept, J = 6.7 Hz, 1H, dipp-CH), 1.11 (d, J = 6.6 Hz, 3H, dipp-CH_3), 1.02 (d, J = 6.8 Hz, 3H, dipp-CH_3), 0.70 (d, J = 6.8 Hz, 3H, dipp-CH_3), 0.41 (d, J = 6.8 Hz, 3H, dipp-CH_3). ^{13}C NMR (126 MHz, d_8-toluene): δ 170.8 (C=N), 163.7 (C–O), 150.7 (C–N), 141.3, 140.6 (dipp–Ar), 136.2, 133.5, 127.5

(Ar–C), 126.0 (dipp–Ar), 124.4 (Ar–C), 124.4, 123.2 (dipp–Ar), 115.1 (Ar–C), 29.43, 28.35 (dipp-CH), 26.57, 26.13, 23.38, 21.77 (dipp-CH_3). ^{7}Li NMR (194 MHz, d_8-toluene): δ 2.16. Elemental Analysis Calculated for $C_{19}H_{21}ClLiNO$ (321.77 g mol^{-1}): C 70.92, H 6.58, N 4.35. Found: C 70.92, H 6.69, N 4.18. MALDI-ToF-MS: *m/z* $[M+H]^+$: 322.20 calculated $[M+H]^+$: 322.15.

Complex **Li6**: (149 mg, 84.7 %) ^{1}H NMR (500 MHz, d_8-THF): δ 8.02 (s, 1H, N=CH), 7.02 (d, $J=3.0$ Hz, 1H, ArH), 6.93 (dd, $J=8.9$, 2.9 Hz, 1H, ArH), 6.45 (d, $J=8.9$ Hz, 1H, ArH), 3.28 (s, 3H, CH_3). ^{13}C NMR (126 MHz, d_8-THF): δ 167.8 (C=N), 162.1 (C–O), 134.3, 132.5, 124.5, 122.8 (Ar–C), 48.30 (CH_3). ^{7}Li NMR (194 MHz, d_8-THF): δ 1.01. Elemental Analysis Calculated for $C_8H_7ClLiNO$ (175.54 g mol^{-1}): C 54.74, H 4.02, N 7.98. Found: C 54.77, H 4.13, N 7.94. MALDI-ToF-MS: *m/z* $[M+H]^+$: 176.06 calculated $[M+H]^+$: 176.04.

Complex **Li7**: (300 mg, 93.1 %) ^{1}H NMR (500 MHz, d_8-toluene): δ 7.56 (s, 1H, N=CH), 6.99-6.97 (m, 3H, dipp-CH), 6.88 (d, $J=2.8$ Hz, 1H, ArH), 6.73 (dd, $J=8.7$, 2.8 Hz, 1H, ArH), 6.40 (d, $J=8.8$ Hz, 1H, ArH), 2.43 (hept, $J=6.8$ Hz, 2H, CH), 0.87 (d, $J=6.8$ Hz, 6H, dipp-CH_3), 0.63 (d, $J=6.8$ Hz, 6H, dipp-CH_3). ^{13}C NMR (126 MHz, d_8-toluene): δ 170.2 (C=N), 166.9 (C–O), 150.1 (C–N), 139.4 (dipp–Ar), 135.9, 135.3 (Ar–C), 123.9, 123.7 (dipp–Ar), 123.4, 120.6, 101.0 (Ar–C), 29.0 (dipp-CH), 25.9, 22.4 (dipp-CH_3). ^{7}Li NMR (194 MHz, d_8-toluene): δ 1.61. Elemental Analysis Calculated for $C_{19}H_{21}ClLiNO$ (321.77 g mol^{-1}): C 70.92, H 6.69, N 4.18. Found: C 69.80, H 7.07, N 4.55. MALDI-ToF-MS: *m/z* $[M+H]^+$: 322.13 calculated $[M+H]^+$: 322.15.

Deposition Numbers 2046461 (for **Li4**), 2046462 (for **Li2**), 2046643 (for {**Li7**}$_4$•2toluene), 2046464 (for **Li3**), 2046465 (for **Li5**), 2046466 (for **Li1**), 2046467 (for {**Li7**}$_4$•toluene), and 2046468 (for **Li7**•THF) contain the supplementary crystallographic data for this paper. These data are provided free of charge by the joint Cambridge Crystallographic Data Centre and Fachinformationszentrum Karlsruhe Access Structures service www.ccdc.cam.ac.uk/structures.

Acknowledgements

We gratefully acknowledge the University of Edinburgh Principal's Career Development PhD Scholarship for funding. J. A. G. also acknowledges the UKRI Future Leaders Fellowship (Grant MR/T042710\1), British Royal Society (Grant RSG\R1\180101), L'Oréal-UNESCO for Women in Science Fellowship and the British Ramsay Memorial Trust for funding. Synchrotron data were collected remotely at beam line I-19 of Diamond Light Source (award CY22240).[65]

Conflict of Interest

The authors declare no conflict of interest.

Keywords: Ligand design · Lithium · Reaction mechanisms · Ring-opening polymerization · Substituent effects

[1] rsc.li/sustainable-plastics-report, *Science to Enable Sustainable Plastics – A White Paper from the 8th Chemical Sciences and Society Summit (CS3)*, **2020**.
[2] J. N. Hahladakis, C. A. Velis, R. Weber, E. Iacovidou, P. Purnell, *J. Hazard. Mater.* **2018**, *344*, 179–199.
[3] F. Shewmaker, M. J. Kerner, M. Hayer-Hartl, G. Klein, C. Georgopoulos, S. J. Landry, *Protein Sci.* **2004**, *13*, 2139–2148.
[4] X. Zhang, M. Fevre, G. O. Jones, R. M. Waymouth, *Chem. Rev.* **2018**, *118*, 839–885.
[5] A. Duda, S. Penczek, *Polimery* **2018**, *48*, 16–27.
[6] F. Nederberg, E. F. Connor, M. Möller, T. Glauser, J. L. Hedrick, *Angew. Chem. Int. Ed.* **2001**, *40*, 2712–2715; *Angew. Chem.* **2001**, *113*, 2784–2787.
[7] N. E. Kamber, W. Jeong, R. M. Waymouth, R. C. Pratt, B. G. G. Lohmeijer, J. L. Hedrick, *Chem. Rev.* **2007**, *107*, 5813–5840.
[8] M. Savioli Lopes, A. L. Jardini, R. Maciel Filho, *Procedia Eng.* **2012**, *42*, 1402–1413.
[9] I. K. Varma, A. C. Albertsson, R. Rajkhowa, R. K. Srivastava, *Prog. Polym. Sci.* **2005**, *30*, 949–981.
[10] G. Montaudo, M. S. Montaudo, C. Puglisi, F. Samperi, N. Spassky, A. LeBorgne, M. Wisniewski, *Macromolecules* **1996**, *29*, 6461–6465.
[11] Z. Zhong, P. J. Dijkstra, J. Feijen, *J. Am. Chem. Soc.* **2003**, *125*, 11291–11298.
[12] P. Hormnirun, E. L. Marshall, V. C. Gibson, A. J. P. White, D. J. Williams, *J. Am. Chem. Soc.* **2004**, *126*, 2688–2689.
[13] A. J. Gaston, G. Navickaite, G. S. Nichol, M. P. Shaver, J. A. Garden, *Eur. Polym. J.* **2019**, *119*, 507–513.
[14] M. Cheng, A. B. Attygalle, E. B. Lobkovsky, G. W. Coates, *J. Am. Chem. Soc.* **1999**, *121*, 11583–11584.
[15] C. K. Williams, L. E. Breyfogle, S. K. Choi, W. Nam, V. G. Young, M. A. Hillmyer, W. B. Tolman, *J. Am. Chem. Soc.* **2003**, *125*, 11350–11359.
[16] C. A. Wheaton, P. G. Hayes, *Catal. Sci. Technol.* **2012**, *2*, 125–138.
[17] B. M. Chamberlain, Y. Sun, J. R. Hagadorn, E. W. Hemmesch, V. G. Young, M. Pink, M. A. Hillmyer, W. B. Tolman, *Macromolecules* **1999**, *32*, 2400–2402.
[18] H. Ma, J. Okuda, *Macromolecules* **2005**, *38*, 2665–2673.
[19] Z. Zhang, X. Xu, W. Li, Y. Yao, Y. Zhang, Q. Shen, Y. Luo, *Inorg. Chem.* **2009**, *48*, 5715–5724.
[20] O. Dechy-Cabaret, B. Martin-Vaca, D. Bourissou, *Chem. Rev.* **2004**, *104*, 6147–6176.
[21] M. J. Stanford, A. P. Dove, *Chem. Soc. Rev.* **2010**, *39*, 486–494.
[22] M. Basko, *Pure Appl. Chem.* **2012**, *84*, 2081–2088.
[23] I. E. Nifant'ev, A. V. Shlyakhtin, A. N. Tavtorkin, P. V. Ivchenko, R. S. Borisov, A. V. Churakov, *Catal. Commun.* **2016**, *87*, 106–111.
[24] J. Xiong, Y. Sun, J. Jiang, C. Chen, X. Pan, C. Wang, J. Wu, *Polyhedron* **2018**, *141*, 118–124.
[25] T. Katsuki, *Coord. Chem. Rev.* **1995**, *140*, 189–214.
[26] C. Gallegos, V. Tabernero, M. E. G. Mosquera, T. Cuenca, J. Cano, *Eur. J. Inorg. Chem.* **2015**, *2015*, 5124–5132.
[27] Z. Liu, H. X. Chen, D. Huang, Y. Zhang, Y. M. Yao, *J. Organomet. Chem.* **2014**, *749*, 7–12.
[28] J. Kasperczyk, M. Bero, *Polymer* **2000**, *41*, 391–395.
[29] P. Kurcok, J. Penczek, J. Franek, Z. Jedliáski, *Macromolecules* **1992**, *25*, 2285–2289.
[30] C.-A. Huang, C.-T. Chen, *Dalton Trans.* **2007**, 5561–5566.
[31] W. Y. Lu, M. W. Hsiao, S. C. N. Hsu, W. Te Peng, Y. J. Chang, Y. C. Tsou, T. Y. Wu, Y. C. Lai, Y. Chen, H. Y. Chen, *Dalton Trans.* **2012**, *41*, 3659–3667.
[32] Z. Cai, D. Xiao, L. H. Do, *J. Am. Chem. Soc.* **2015**, *137*, 15501–15510.
[33] P. Hormnirun, E. L. Marshall, V. C. Gibson, R. I. Pugh, A. J. P. White, *Proc. Nat. Acad. Sci.* **2006**, *103*, 15343–15348.
[34] F. M. García-Valle, R. Estivill, C. Gallegos, T. Cuenca, M. E. G. Mosquera, V. Tabernero, J. Cano, *Organometallics* **2015**, *34*, 477–487.
[35] S. Ghosh, D. Chakraborty, B. Varghese, *Eur. Polym. J.* **2015**, *62*, 51–65.
[36] W. Clegg, M. R. J. Elsegood, "CCDC 1997440," DOI 10.5517/ccdc.csd.cc251hk9, **2020**.
[37] E. Weiss, *Angew. Chem. Int. Ed. Engl.* **1993**, *32*, 1501–1523.
[38] L. Yang, D. R. Powell, R. P. Houser, *Dalton Trans.* **2007**, 955–964.
[39] C. Janiak, *J. Chem. Soc. Dalton Trans.* **2000**, 3885–3896.
[40] C. B. Aakeröy, T. A. Evans, K. R. Seddon, I. Pálinkó, *New J. Chem.* **1999**, *23*, 145–152.
[41] F. Afshar Taromi, B. Notash, M. Nekoomanesh, R. Zahedi, R. Jamjah, G. Zohuri, *Acta Crystallogr. Sect. E* **2012**, *68*, o522–o522.
[42] G. S. Manku, *Theoretical Principles of Inorganic Chemistry*, Tata McGraw-Hill, New Delhi, **1980**.
[43] R. K. Dean, A. M. Reckling, H. Chen, L. N. Dawe, C. M. Schneider, C. M. Kozak, *Dalton Trans.* **2013**, *42*, 3504–3520.
[44] P. L. Antonelli, T. D. Rogers, M. A. Willard, *J. Theor. Biol.* **1973**, *41*, 1–21.
[45] H. J. Reich, *Chem. Rev.* **2013**, *113*, 7130–7178.
[46] C. Chen, Y. Cui, X. Mao, X. Pan, J. Wu, *Macromolecules* **2017**, *50*, 83–96.
[47] L. N. Saunders, L. N. Dawe, C. M. Kozak, *J. Organomet. Chem.* **2014**, *749*, 34–40.

[48] M. A. Nichols, P. G. Williard, *J. Am. Chem. Soc.* **1993**, *115*, 1568–1572.
[49] A. B. Kremer, P. Mehrkhodavandi, *Coord. Chem. Rev.* **2019**, *380*, 35–57.
[50] M. Fernández-Millán, P. Ortega, T. Cuenca, J. Cano, M. E. G. Mosquera, *Organometallics* **2020**, *39*, 2278–2286.
[51] H. Y. Chen, L. Mialon, K. A. Abboud, S. A. Miller, *Organometallics* **2012**, *31*, 5252–5261.
[52] S. C. Roşca, D. A. Roşca, V. Dorcet, C. M. Kozak, F. M. Kerton, J. F. Carpentier, Y. Sarazin, *Dalton Trans.* **2013**, *42*, 9361–9375.
[53] K. M. Osten, P. Mehrkhodavandi, *Acc. Chem. Res.* **2017**, *50*, 2861–2869.
[54] D. C. Aluthge, J. M. Ahn, P. Mehrkhodavandi, *Chem. Sci.* **2015**, *6*, 5284–5292.
[55] R. E. Mulvey, S. D. Robertson, *Angew. Chem. Int. Ed.* **2013**, *52*, 11470–11487; *Angew. Chem.* **2013**, *125*, 11682–11700.
[56] L. M. Alcazar-Roman, B. J. O'Keefe, M. A. Hillmyer, W. B. Tolman, *Dalton Trans.* **2003**, *15*, 3082–3087.
[57] A. Kowalski, A. Duda, S. Penczek, *Macromolecules* **1998**, *31*, 2114–2122.
[58] K. Devaine-Pressing, J. H. Lehr, M. E. Pratt, L. N. Dawe, A. A. Sarjeant, C. M. Kozak, *Dalton Trans.* **2015**, *44*, 12365–12375.
[59] R. Duan, B. Gao, X. Li, X. Pang, X. Wang, H. Shao, X. Chen, *Polymer* **2015**, *71*, 1–7.
[60] N. Ajellal, J. F. Carpentier, C. Guillaume, S. M. Guillaume, M. Helou, V. Poirier, Y. Sarazin, A. Trifonov, *Dalton Trans.* **2010**, *39*, 8363–8376.
[61] E. Fazekas, G. S. Nichol, M. P. Shaver, J. A. Garden, *Dalton Trans.* **2018**, *47*, 13106–13112.
[62] P. Pfeiffer, E. Buchholz, O. Bauer, *J. Prakt. Chem.* **1931**, *129*, 163–177.
[63] G. Occhipinti, V. R. Jensen, H. R. Bjørsvik, *J. Org. Chem.* **2007**, *72*, 3561–3564.
[64] P. A. Nikitina, A. S. Peregudov, T. Y. Koldaeva, L. G. Kuz'Mina, E. I. Adiulin, I. I. Tkach, V. P. Perevalov, *Tetrahedron* **2015**, *71*, 5217–5228.
[65] N. T. Johnson, P. G. Waddell, W. Clegg, M. R. Probert, *Crystals* **2017**, *7*, 360.

Manuscript received: August 12, 2021
Revised manuscript received: September 20, 2021